Capturing aerosol droplets with fibers

R Labbé, Camille Duprat

View Article Online
DOI: 10.1039/C9SM01205B

Journal Name

ARTICLE TYPE

Cite this: DOI: 10.1039/xxxxxxxxxx

Capturing aerosol droplets with fibers†

R. Labbé,[a] and C. Duprat[a]

Received Date
Accepted Date

DOI: 10.1039/xxxxxxxxxx

www.rsc.org/journalname

Capturing droplets from a stream with a fibrous material is a well-known and well-used process, from coalescence filters to fog harvesting. In this paper, we report experimental measurements of collection efficiency with a model system consisting in an array of vertical nylon fibers. In particular, we report precise measurements over a large range of parameters, and identify the key role played by the drop distribution on the overall collection efficiency. Due to a growth and coalescence process, this drop distribution evolves toward a regular pattern of uniformly distributed drops, and a balance between capillarity and gravity sets an average drop size. Accounting for these effects in a simple inertial impaction model allows predictive and quantitative comparisons with experiments. Drop growth can be suppressed by forming long continuous liquid columns between close fibers; incoming droplets immediately coalesce with these wet columns, and the capture efficiency is increased. In addition, we extend our model to take into account the interactions between fibers.

1 Introduction

The passive filtration of liquid droplets from aerosol streams or emulsions is done by placing a porous (generally fibrous) structure in the path of the mist. In particular, coalescence filters are used to remove liquid from aerosols[1–3] or for demulsification[4,5]. Plants can intercept wind-blown water drops from fog with their leaves; this so-called *cloud water interception* can have a significant impact on the water balance in arid or semi-arid regions as fog water is redirected to the ground[6,7] and certain plants rely on intercepted fog water as their main or sole source of water[8,9]. For a couple of decades, *fog harvesting*, i.e. the collection of fresh water from fog, has been developed for domestic use or for agriculture/livestock, as well as for reforestation projects[10–12]. As in coalescence filters, the fog droplets are captured as they impact the wires of fibrous nets; the water is then collected as drops fall along the mesh.

The main mechanisms for this removal of droplets from gas or liquid streams are inertial impaction and interception, while other mechanisms (gravitational, brownian or electrostatic effects) may play a role in specific systems[1]. Despite extensive literature on aerosol filtration and fog harvesting, there is a lack of measurements on model systems. Numerous studies aim at optimizing the collection efficiency; however, developed models are mostly empirical, and therefore only applicable to specific fibrous materials and operating conditions. A simple inertial impaction model was proposed by Langmuir and Blodgett[13]; this model is currently widely used, although there are few direct comparisons with experiments. Wong et al.[14] report experiments on a model system consisting in a controlled sulfuric acid aerosol projected onto parallel metallic wires; these measurements are not in agreement with the model[13], and the reason of this discrepancy remains unclear.

In this paper, we report experimental measurements and theoretical predictions of aerosol collection efficiency with an idealized model system consisting in an array of vertical nylon fibers.

2 Experiments

In order to obtain a controlled and well characterized mist, we use a custom made environmental wind tunnel (Fig. 1(a)). The tunnel contains a large turbulent chamber in which a water bath is maintained at constant height; piezoelectric actuators vibrating at ultrasonic frequencies excite the water surface to emit micron-sized droplets. Fans are used to create turbulence, ensuring an homogeneous mixing of the water droplets within the air stream. The mist is then pushed through an honeycomb structure and convergent in order to obtain an homogenous, laminar and well controlled flow of fog through an exit vein of surface area $S_{wt} = 22 \times 22$ cm^2. The water flow rate is kept constant $Q_w = 7\text{Lh}^{-1}$, corresponding to fog water content (i.e. density) between 4 and 20 gm^{-3}, and the average flow velocity can be adjusted to $2 < U < 10$ m.s^{-1}. We use a microscope objective

[a] *LadHyX, Department of Mechanics, CNRS, École polytechnique, 91128 Palaiseau, France*

† Electronic Supplementary Information (ESI) available: [details of any supplementary information available should be included here]. See DOI: 10.1039/b000000x/

‡ Additional footnotes to the title and authors can be included *e.g.* 'Present address:' or 'These authors contributed equally to this work' as above using the symbols: ‡, §, and ¶. Please place the appropriate symbol next to the author's name and include a `\footnotetext` entry in the the correct place in the list.

View Article Online
DOI: 10.1039/C9SM01205B

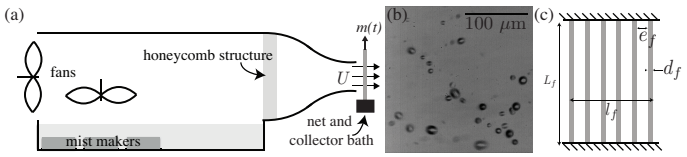

Fig. 1 (a) Sketch of the mist-wind tunnel. (b) Picture of the fog at the exit of the wind tunnel. (c) Ideal net.

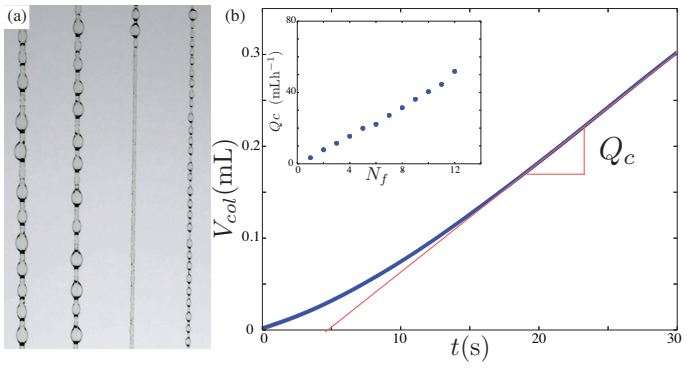

Fig. 2 (a) Collection of droplets on the net, for fiber diameters d_f (from left to right) 800, 600, 300 and 85 μm. (b) Evolution of the volume of collected water V_{col} with time, for a net composed of fibers of diameter $d_f = 300$ μm. The slope gives the collection flow rate Q_c. Inset: evolution of Q_c with the number of fibers in the net N_f.

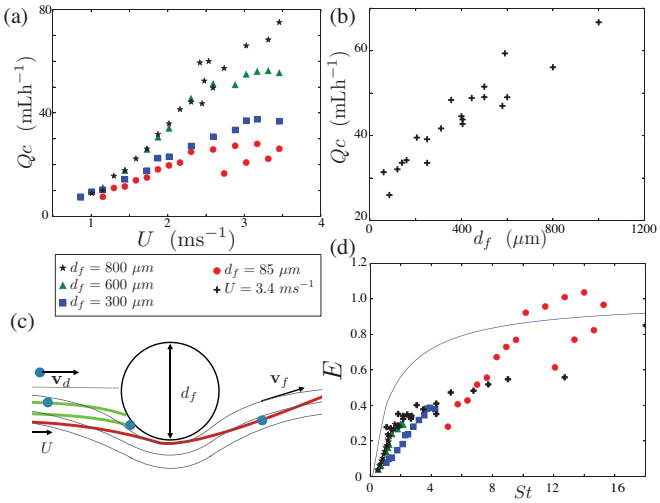

Fig. 3 Collection flow rate Q_c for a net of 10 fibers, as (a) a function of the mist velocity U and diameter $d_f = 800$ μm (black stars), $d_f = 600$ μm (green triangle), $d_f = 300$ μm (blue square) and $d_f = 85$ μm (red dots) and (b) as a function of the fiber diameter d_f for a velocity $U = 3.4$ ms^{-1} (black crosses). (c) Sketch of droplets trajectories in a flow around a fiber. (d) Efficiency as a function of Stokes number. Experimental data (symbols) and solution (5-7) (solid curve).

mounted on a fast camera (with a long distance optical adaptor) to image the fog and measure the droplets radii (Fig. 1(b)). The droplet distribution is narrow, with a droplet radius $r_d = 3 \pm 3$ μm inside the wind tunnel, and we estimate a larger average value of 4μ m at the exit due to coalescences, as will be detailed in the following. These characteristics are close to environmental fog conditions and filtration operating conditions[1,10]. A collecting net composed of N_f vertical parallel nylon fibers of diameters $60 < d_f < 2000$ μm is placed at the exit and spans the entire vein in height, i.e. the fiber length is $L_f = 22$ cm (Fig. 1(c)). We define the total projected surface of the net as $S_f = N_f L_f d_f$. Water wets partially the nylon, with a contact angle hysteresis $\Delta\cos\theta = \cos\theta_a - \cos\theta_r = 0.23$ (measured with a tensiometer). The net is maintained by a structure with a collector bath, and the distance between the fibers e_f can be accurately adjusted. This structure (net and collector bath) is attached to a strain captor that measures the evolution of collected water mass, both on the fibers and in the collecting bath, as a function of time. A reference net composed of 10 fibers of radius $r_f = 300$ μm, corresponding to a surface $S_f = 660$ mm^2, is placed in the wind tunnel for all experiments; the collection rate of this reference net is used to ensure constant fog properties and is checked to be constant over the course of all experiments.

As the mist passes through the mesh, fog droplets starts collecting on the fibers (Fig. 2(a)); drops appear on the fibers, grow, coalesce and fall periodically, and water accumulates in the bath. By convention, we use *droplet* for the suspended fog droplets and *drop* for the sessile drops on the fiber. The typical evolution of mass with time is given in Fig. 2 (b). As the flow of fog starts, we first observe a short transient regime (~ 15 s) where the first drops appear on the fibers. After this short initial wetting of the fibers, drops fall continuously and the volume of collected water increases linearly with time, i.e. the collection rate Q_c is constant. While at short time scale the collection is discontinuous, i.e. is given by the successive fall of individual drops, over the time scale of the experiment (up to 30 minutes) the flow rate remains remarkably constant, indicating that drops fall freely under gravitational drainage and do not accumulate on the wires, i.e. drainage is not a limiting factor here. We can thus define the collection efficiency E as the ratio of the collected flow of water Q_c to the flow of water passing through the net $Q_w S_f / S_{wt}$, i.e.

$$E = \frac{Q_c S_{wt}}{Q_w S_f}. \quad (1)$$

3 Collection mechanisms

We first focus on widely spaced fibers ($e_f = 5$ mm), i.e. on the collection efficiency of a single fiber. Measurements are performed on $N_f = 15$ evenly spaced fibers; the experiments is repeated 12 times, each time removing one fiber from the net. The collection rate is proportional to N_f (inset in Fig. 2(b)); we thus verify that the fibers are independent, i.e. neighbour fibers are not affecting the collection rate of a single fiber. We measure this collection rate for various mean flow velocity U (Fig. 3 (a)) and fibers diameters d_f (Fig. 3 (b)). The collection rate, i.e. the collection efficiency, increases with the fibers diameter and fluid velocity.

The main mechanism for the collection is the inertial impact of droplets on the fibres: a droplet carried in the flow can either follow the streamlines, and avoid the obstacle, or impact the fiber provided it has enough inertia (Fig. 3 (c)). With typical flow speeds U of 1 m/s, fiber radius of typically 100 μm

View Article Online
DOI: 10.1039/C9SM01205B

gives a moderate Reynolds number for the flow around a fiber ($Re_f \sim 100$), whereas the Reynolds number based on droplets is about $Re_d \sim 0.1$ so the motion of the drop is dominated by viscous drag. The motion of the fog droplet is thus given by a balance between viscous drag and inertia, i.e.

$$m_d \frac{\mathrm{d}\mathbf{v_d}}{\mathrm{dt}} = -6\pi\mu r_d(\mathbf{v_d} - \mathbf{v_f}) \tag{2}$$

where $\mathbf{v_d}$ is the droplet velocity, $\mathbf{v_f}$ the flow velocity, $m_d = (4/3)\rho_d \pi r_d^3$ the mass of the droplet and μ the viscosity of air. Adimensionalizing this equation with the mean flow velocity U and the characteristic flow time scale $t_f = \frac{d_f}{2U}$, we obtain the evolution equation (bars denote dimensionless values)

$$\frac{\mathrm{d}\bar{\mathbf{v}}_\mathbf{d}}{\mathrm{d}\bar{t}} = \frac{1}{St}(\bar{\mathbf{v}}_\mathbf{d} - \bar{\mathbf{v}}_\mathbf{f}) \tag{3}$$

with a single parameter, the Stokes number

$$St = \frac{4\rho_d r_d^2 U}{9\mu d_f}, \tag{4}$$

that corresponds to the ratio of inertial force to viscous drag. The trajectory of the droplet, and thus the condition for impact and the collection rate, depends only on the Stokes number. At large Stokes numbers, inertia dominate and droplets can not follow curved streamlines, thus impacting the fiber. At small Stokes, all droplets follow the streamlines and are thus deviated around the fiber, and the collection rate is null. The efficiency E can be linked to the drops trajectories, by assuming that all drops impacting the fibers are collected; we thus have a unique value of E for a given Stokes number, and the efficiency increases with increasing impacts, thus increasing Stokes numbers. Solving equation (3) requires to know the flow field around the fiber. We assume the flow is potential, and solve numerically for the drop trajectories. A first solution of this problem was given by[13], who gave an approximate solution as

$$E = 0 \quad \text{for } St < 0.125 \tag{5}$$

$$E = 0.466\ \mathrm{Log}_{10}(8\mathrm{St})^2 \quad \text{for } 0.125 < \mathrm{St} < 1.1 \tag{6}$$

$$E = \frac{St}{St + \pi/2} \quad \text{for } St > 1.1. \tag{7}$$

We plot our data as a function of Stokes number (Fig. 3 (d)), alongside the solution (5-7). The fog droplet radius here is taken as the average value $r_d = 3.9\mu$m. The data do not collapse onto a single curve; in addition, the solution (5-7) overestimates the efficiency. Note that a small error in r_d gives rise to a large variation of St; the experimental data all fall within an error of $\pm 3\mu$m, consistent with the measured drop size distribution. However, we observe coherent trends and the discrepancy can not simply be explained with a large droplet distribution.

The main limitation of this model is that it does not account for the growth of drops on the fiber; however, drops can reach a size larger than the fiber diameter (Fig. 2(a)) and the collection is slower in the transient regime when no drops exist on the fiber (Fig. 2). We thus expect that the drops sizes and distribution play a major role in the flow deviation and the impact and coalescence of incoming droplets, thus on the overall efficiency.

Initially, there are no drops on the fiber. Since the fog is homogeneous, droplets impact anywhere on the fiber, resulting in an even distribution of small drops along the fiber length. Incoming droplets coalesce with existing drops, and two adjacent drops may coalesce to form a larger drop. Drops on the fibers thus grow with time, until they reach a critical size where they fall; as they fall, they entrain the drops placed below them on the fibers (see video in Supplementary Material). This process is repeated periodically. We simulate this drop growth numerically in 1D with an iterative algorithm (coded in Python). At each time step, droplets impact the fiber uniformly; as two drops touch, they merge and their center of mass is displaced. The drop fall when reaching a critical drop size, clearing the fiber of all drops present below. At each time, we report the number N of drops on the fiber (Fig. 4 (a)). Gradually, after a short time where a large number of small drops are evenly distributed on the fiber, a regular droplet pattern is formed: for most of the collection process there is a constant number N_d of drops equally distributed along the fiber, as seen in the drop number distribution (inset of Fig. 4 (b)) and as also observed in the experiments (Fig. 4 (e)). Drops are separated by a distance close to the typical drop size $2\ell_c$, i.e. $N_d = \frac{L_f}{2\ell_c}$. This value is nearly independent of the fiber radius (Fig. 4 (b)). The process is reminiscent of breath patterns, i.e. the growth and coalescence observed in condensation[15,16] and in the de-emulsification, i.e. the collection of suspended droplets in a flow on an horizontal fiber[4] where similar algorithms have been used. Similarly, the combined growth and merging process leads to a constant coverage of the surface; the main difference here is the maximal drop size above which drops fall that sets a mean drop size along the fibers. This critical, or maximum drop size is given by a balance between surface tension and weight. Assuming that the force maintaining the drop is given by $\pi d_f \gamma \Delta \cos\theta$[17], and considering a spherical drop of volume $V_d = \frac{4}{3}\pi R_{df}^3$, the maximum drop size is given by

$$R_{df} = \left(\frac{3}{4}\ell_c^2 \Delta\cos(\theta) d_f\right)^{1/3} \tag{8}$$

with $\ell_c = \sqrt{\frac{\rho g}{\gamma}}$ the capillary length. We perform measurements of this critical value on an independent set-up, where mist is projected through a small tube on a single fiber and the evolution of the drop size is recorded from the side. We verify the expression (8) for several fiber radii (Fig. 4 (c)). While the drop radius always slowly evolves in time due to the constant coalescences of incoming droplets, size distributions over several cycles reveal that there is statistically an average drop size, set by R_{df} (inset of Fig. 4 (c)).

We can thus consider that there is on average a constant number of drops N_d of size R_{df} on the fiber. We assume that all collection occurs on the drops, i.e. the characteristic length for the flow time scale as well as the collection surface is now R_{df} rather than r_f. We thus defined a modified Stokes number

$$St_{drop} = St\frac{d_f}{2R_{df}}. \tag{9}$$

View Article Online
DOI: 10.1039/C9SM01205B

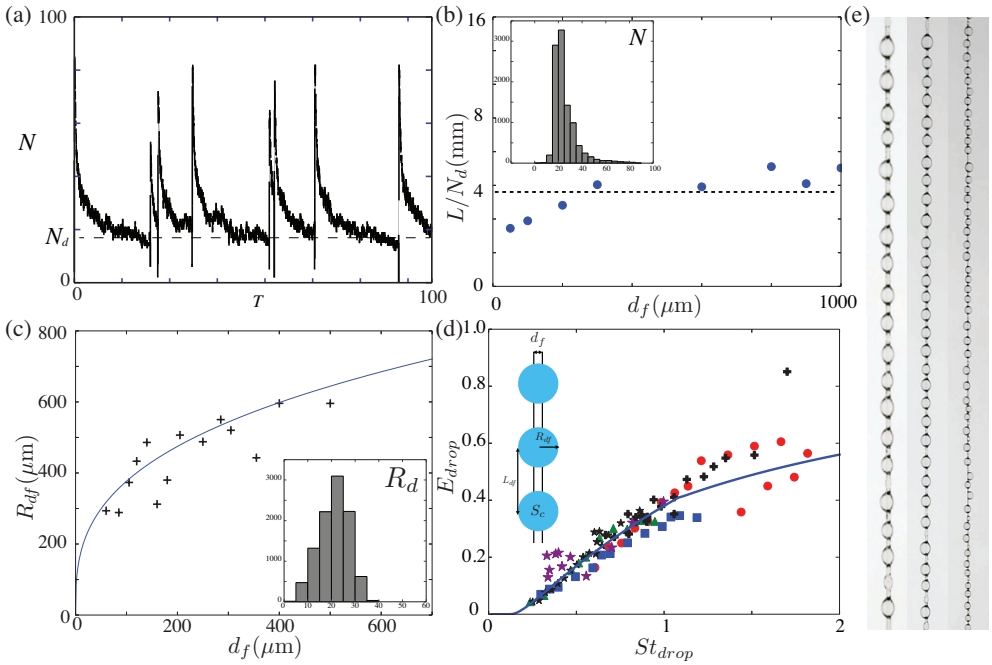

Fig. 4 (a) Evolution of the number of drops on the fibers obtained numerically. (b) Evolution of the final distance between drops as a function of the fiber radius. Inset: histogram of the number of drops N over several cycles. (c) Evolution of the maximum drop size as a function of the fiber radius; solid curve: equation (8). Inset: histogram of the drops sizes R_d over several cycles. (d) Collection efficiency E as a function of the modified Stokes number St_{drop}. Symbols correspond to the data presented in Fig. 3, with the addition of efficiency measured for inclined fibers at different angles α, with $d_f = 300$ μm and a velocity of $U = 3$ ms^{-1} (stars). Solid curve is the solution (5-7). (e) Drop distributions observed experimentally on fibers of radius (from left to right) 600, 300 and 85 μm.

The collection efficiency is the efficiency E associated with this modified Stokes number, renormalized by the ratios of collection areas i.e.

$$E_{drop} = E\frac{S_f}{S_{df}} \tag{10}$$

where $S_{df} = N_d \pi R_{df}^2$ is the projected surface of the drops. We plot our data with these two new parameters E_{drop} and St_{drop} (Fig. 4(d)). All data now collapse onto a single curve, indicating that the relevant parameters indeed are the ones coming from the proposed drop distribution. The dependence in fiber radius is well captured through the dependance of the mean drop size R_{df}. In addition, the solution (5-7) is in good agreement with the experimental data. Note that here again the droplet radius is taken as a constant $r_d = 3.9$ μm, in agreement with the value expected at the exit of the vein. The small spreading of the data corresponds to errors in Stokes number of about 15%, that is a spread in droplet radius below 4%, which is below the width of the droplet size distribution.

We further validate this model by modifying the maximal size R_{df} of the drops. This can be done, without changing the fiber radius and surface properties or the flow, by inclining the fibers by an angle α : small α (horizontal) fibers can hold larger drops than large α (vertical) fibers[18,19]. We measure experimentally the maximal drop size that can be held by an inclined fiber with our independent setup (see Supplementary material). This size is used to evaluate the efficiency and the Stokes number (stars in Fig. 4(c)). The data collapse on the curve obtained for vertical

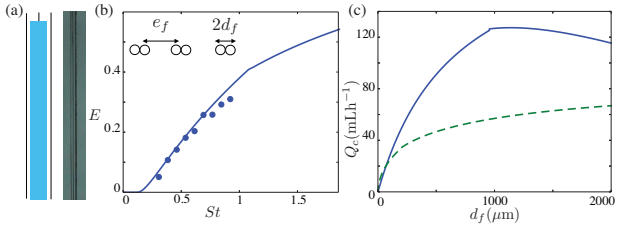

Fig. 5 (a) Sketch and photography of two fibers collapsed by a capillary bridge, placed in the mist, on which no drop growth is observed as all droplets coalesce immediately with the column. (b) E as the function of the Stokes number St. Experimental data for two fibers of 300 μm. The solid curve corresponds to (5-7) for a cylinder of diameter $2d_f$. Inset: Sketch of the fibers repartition. (c) Comparison of the collected flow rate for wet columns (solid line) and fibers in partial wetting (dashed line) of equivalent diameter.

View Article Online
DOI: 10.1039/C9SM01205B

fibers. Scatter is more pronounced for small angles α, i.e. small Stokes numbers, as the drops hanging on horizontal fibers more resemble an assembly of spheres than a cylinder, which modifies equations (5-7). A detailled calculation and comparison to experimental data is given in the Supplementary material. Another way to affect the drop distribution is to change the contact angle hysteresis $\gamma\Delta\cos(\theta)$. In particular, making the fibers perfectly hydrophilic will suppress the presence of drops on the fibers, that will thus behave as totally wet cylinders. This effect can actually be obtained by using two fibers separated by a small distance $e_f < d_f$ (Fig. 5(a)); indeed, the liquid will spread between the fibers and form a long liquid column[20] (see Fig. 5 in Supplementary material). As droplets impact this liquid column, they immediately coalesce and are drained continuously. We thus suppress the drop growth on the fibers, and simply have a wet cylinder of diameter $2d_f$. The measured efficiency is then in excellent agreement with the model (5-7), i.e. the model without drop growth (Fig.5(b)). Note that we used here the value $r_d = 3.9\ \mu$m that was treated as an adjustable parameter beforehand, thus validating our choice of parameter which simply reflects on the more probable droplet size of our experimental fog. We can compare the collection rate of a net composed of independent fibers, i.e. with drop growth, to the collection rate of a net with a fiber arrangement with liquid columns (Fig.5(c)). For a given fiber radius, the collection rate is always significantly higher on the columns than on the partially wetting fibers.

4 Collection efficiency of a net

In order to define the efficiency of a net, and not only of a single fiber, we next evaluate the collection rate of an assembly of fibers, with varying inter-fiber distances e_f, for a given surface S_m. We report the collection efficiency of a single fiber within this assembly E, or equivalently Q_c/N_f (Fig. 6 (a-b)). At large distances e_f, the fiber collection rate is constant and equal to the single fiber collection rate defined for independent fibers. Below a critical distance, the fiber collection rate decreases to reach 0 when the fibers are touching, i.e. $e_f = d_f$. This decrease of collection rate can be accounted for by a decrease in flow speed through the net as the permeability decreases. Following a simple model[21] we estimate the pressure drop through the mesh by considering a drag force on each fiber

$$F = \frac{1}{2}\rho C_d d_f L_f U^2 \tag{11}$$

where C_d is a drag coefficient and is treated as an adjustable parameter. We can thus write for the momentum p

$$\frac{\mathrm{d}p}{\mathrm{d}t} = L_f \ell_f \rho (U^2 - U_{acr}^2) = N_f F, \tag{12}$$

such that, with $\ell_f = N_f e_f$, the velocity across the net is given by

$$U_{acr} = U\sqrt{1 - \frac{C_d d_f}{2e_f}}. \tag{13}$$

When $e_f = d_f$, no fluid passes through the net, i.e. $U_{acr} = 0$, while when $e_f \gg d_f$, $U_{acr} \simeq U$. Accounting for this change in velocity,

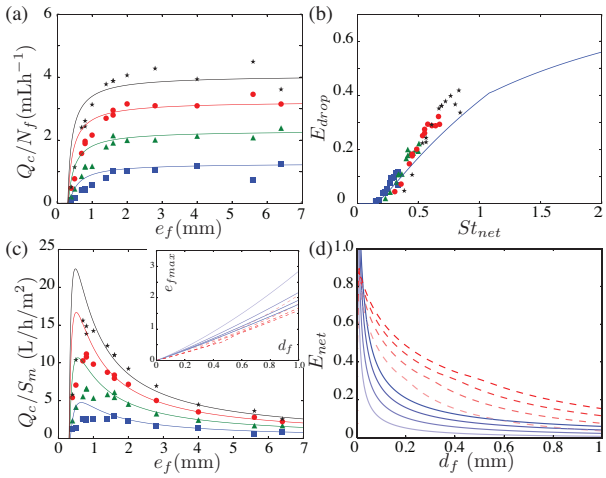

Fig. 6 (a) Collection of one fiber as a function of e_f, for a mesh of width 22 mm with fibers of diameter 300 μm and a velocity $U = 1.15$ ms^{-1} (blue), $U = 1.7$ ms^{-1} (green), $U = 2.3$ ms^{-1} (red) and $U = 2.8$ ms^{-1} (black). Experimental data (points) and curves derived from equations (5-7) and (13). (b) Efficiency of a single fiber in the net as a function of the modified Stokes number. Line: equations (5-7) and (13) with $C_d = 1$. (c) Collection of a net as a function of e_f. Inset: Evolution of e_{fmax} as a function of the diameter d_f. (d) Maximal efficiency of a net at the optimal fiber spacing e_{fmax} as a function of the fiber diameter for different flow velocity, for perfectly hydrophilic fibers (red dashed line) and partially wetting fibers (blue plain line).

we define a new Stokes number St_{net} for a porous net

$$St_{Net} = St_{drop} U_{acr}/U. \tag{14}$$

The efficiency E of one fiber in the net is thus given by the efficiency at the modified Stokes number (Fig. 6 (b)). All data collapse together and are well described with equations (5-7) and a drag coefficient $C_d = 1$. The prediction for the collection rate accurately describe the experimental results (Fig. 6 (a)). To refine the model we could take into account the presence of drops on the fibers, which increases the drag[22]. In addition, we slightly overestimate the collection rate as we assume no finite size effect, i.e. we consider that all the fog goes through the net. However, the deviation of fog around the net is important, in particular for small spacings (low permeability).

We define the overall efficiency of the net E_{net} with the collection per unit area Q_c/S_m (Fig. 6 (c)). While decreasing the fiber collection efficiency, decreasing the distance between adjacent fibers also increases the number of fibers per unit area, and thus increase the overall collection of the net. There is thus an optimal value for collection, independent of the velocity, corresponding to the maximal number of fibers that can be placed in the net without a decrease in single fiber collection rate. The overall efficiency of the net is the efficiency E_{net} associated with the modified Stokes number St_{net}, and renormalized by the ratios of areas, i.e.

$$E_{net} = E\frac{NS_f}{S_{net}}. \tag{15}$$

For a given fiber radius and wetting properties, we obtain the optimal distance e_f, i.e. the distance at which E_{net} is the maximal, as

View Article Online
DOI: 10.1039/C9SM01205B

shown in the inset in Fig. 6(c). The optimal distance increases linearly with fiber radius, and remains close to $e_{fmax} = 2d_f$. Finally, we plot the net efficiency E_{net} at the optimal distance e_{fmax} as a function of the fiber radius, and for various incoming velocities and wetting properties, either in partial wetting and a uniform drop distribution or for totally wetting, i.e. no drop growth, in Fig. 6(d). The net efficiency increases with decreasing fiber diameter as the number of fibers per surface area increases. The divergence of efficiency at small diameters in partial wetting is unphysical; indeed, we have to take into account that for small diameters the size of the drops become comparable to the inter-fiber distance, i.e. $e_{fmax} \simeq 2d_f \simeq R_{df}$, leading to the formation of bridges between adjacent fibers and ultimately clogging of the net.

5 Conclusions

In conclusion, the collection rate on a single fiber strongly depends on the drop distribution on the fiber. This distribution remarkably evolves towards a uniform pattern of a constant number of evenly distributed drops whose size is set by a balance between gravitational and surface tension forces, and is thus strongly affected by the wetting properties of the fibers. Collection can be affected by small changes in drop size (e.g. with a small inclination of the fibers or a change in contact angle hysteresis). A small change in the structure of the net allows to create superhydrophilic fibers by simply bringing adjacent fibers closer in order to form continuous liquid columns; the overall efficiency is then significantly increased. The collapse of adjacent fibers to form these columns may be easily induced by using flexible fibers[23–26]. In addition, in this model system, the liquid can freely flow along the fibers which prevents clogging, i.e. the accumulation of drops on the wires that may block the flow and affect the collection. Indeed, limited drainage is though to be a major limiting factor in collection efficiency, as it causes an increase in pressure drop[27,28] and/or deviation of the droplets[29]. These studies suggest that the optimal collection results from a compromise between favorable drainage, to prevent clogging, and adhesion on the fibers, to avoid re-entrainment of the droplets in the flow. This particular situation is obtained when the drops exhibit both a low contact angle and a small contact angle hysteresis, which requires specific surface treatments[29], and large scale measurements do not show significant differences in collection efficiency with such meshes[30]. In comparison, nets composed of vertical parallel fibers seem to yield a higher collection rate even in partial wetting situations[25,26,31]. The results presented here may be used to derive design rules for the optimisation of aerosol collection with such fibrous materials.

Conflicts of interest

There are no conflicts to declare.

Acknowledgements

Notes and references

1 R. Mead-Hunter, A. J. King and B. J. Mullins, *Separation and Purification Technology*, 2014, **133**, 484–506.
2 K. Zhang, F. Liu, A. J. Williams, X. Qu, J. J. Feng and C.-H. Chen, *Physical review letters*, 2015, **115**, 074502.
3 R. Zhang, B. Liu, A. Yang, Y. Zhu, C. Liu, G. Zhou, J. Sun, P.-C. Hsu, W. Zhao, D. Lin *et al.*, *Nano letters*, 2018, **18**, 1130–1138.
4 B. J. Briscoe, K. P. Galvin, P. F. Luckham and A. M. Saeid, *Colloids and Surfaces*, 1991, **56**, 301–312.
5 R. Wahi, L. A. Chuah, T. S. Y. Choong, Z. Ngaini and M. M. Nourouzi, *Separation and Purification Technology*, 2013, **113**, 51–63.
6 L. Bruijnzeel *et al.*, *Land use and water resources research*, 2001, **1**, 1–1.
7 A. Pryet, C. Domínguez, P. F. Tomai, C. Chaumont, N. D'Ozouville, M. Villacís and S. Violette, *Agricultural and Forest Meteorology*, 2012, **161**, 94–106.
8 P. W. Rundel, B. Palma, M. . Dillon, M. R. Sharifi, E. T. Nilsen, K. Boonpragob and J. R. Gutierrez, *Re vista Chilena de Historia Natural*, 1997, **70**, 341–349.
9 Z. Pan, W. G. Pitt, Y. Zhang, N. Wu, Y. Tao and T. T. Truscott, *Nature plants*, 2016, **2**, 16076.
10 R. S. Schemenauer and P. I. Joe, *Atmospheric Research*, 1989, **24**, 53–69.
11 O. Klemm, R. S. Schemenauer, A. Lummerich, P. Cereceda, V. Marzol, D. Corell, J. Van Heerden, D. Reinhard, T. Gherezghiher, J. Olivier, P. Osses, J. Sarsour, E. Frost, M. J. Estrela, J. A. Valiente and G. M. Fessehaye, *Ambio*, 2012, **41**, 221–234.
12 7th International Conference on Fog, Fog Collection and Dew, 2016.
13 I. Langmuir and K. Blodgett, *Mathematical investigation of water droplet trajectories*, 1945.
14 J. B. Wong, W. E. Ranz and H. F. Johnstone, *Journal of Applied Physics*, 1955, **26**, 244–249.
15 B. Derrida, C. Godreche and I. Yekutieli, *Phys. Rev. A*, 1991, **44**, 6241–6251.
16 D. Fritter, C. M. Knobler and D. A. Beysens, *Physical Review A*, 1991, **43**, 2858–2870.
17 E. Lorenceau, T. Senden and D. Quéré, *Molecular Gels: Materials with Self-Assembled Fibrillar Networks*, 2006, 223–237.
18 B. J. Mullins, I. E. Agranovski, R. D. Braddock and C. M. Ho, *Journal of Colloid and Interface Science*, 2004, **269**, 449–458.
19 Z. Huang, X. Liao, Y. Kang, G. Yin and Y. Yao, *Journal of colloid and interface science*, 2009, **330**, 399–403.
20 S. Protiere, C. Duprat and H. Stone, *Soft Matter*, 2013, **9**, 271–276.
21 J. d. D. Rivera, *Atmospheric Research*, 2011, **102**, 335–342.
22 A. A. Kirsch, *Journal of Colloid And Interface Science*, 1978, **64**, 120–125.
23 C. Duprat, S. Protière, A. Beebe and H. Stone, *Nature*, 2012, **482**, 510–513.
24 C. Duprat and S. Protiere, *EPL*, 2015, **111**, 56006.
25 C. Duprat, R. Labbe and A. Rewakowicz, Fluid and Elasticity 2015, Biarritz, France, 2015.

View Article Online
DOI: 10.1039/C9SM01205B

26 A. Rewakowicz, J. M. Chomaz and C. Duprat, 7th International Conference on Fog, Fog Collection and Dew, 2016.

27 T. Frising, D. Thomas, D. Bémer and P. Contal, *Chemical Engineering Science*, 2005, **60**, 2751–2762.

28 P. Contal, J. Simao, D. Thomas, T. Frising, S. Callé, J. C. Appert-Collin and D. Bémer, *Journal of Aerosol Science*, 2004, **35**, 263–278.

29 K. C. Park, S. S. Chhatre, S. Srinivasan, R. E. Cohen and G. H. McKinley, *Langmuir*, 2013, **29**, 13269–13277.

30 D. Fernandez, A. Torregrosa, P. Weiss, R. Cohen, D. Sorensen, J. Kleingartner, G. McKinley, A. Mairs, S. Wilson, M. Bowman, T. Barkley and M. Gravelle, 7th International Conference on Fog, Fog Collection and Dew, 2016.

31 W. Shi, M. J. Anderson, J. B. Tulkoff, B. S. Kennedy and J. B. Boreyko, *ACS applied materials & interfaces*, 2018.